Bioinspired micrograting arrays mimicking the reverse color diffraction elements evolved by the butterfly Pierella luna

Bio-inspired micro-grating arrays: mimicking the reverse color diffraction elements evolved by the butterfly Pierella luna

Grant England[*], Mathias Kolle[*†§], Philseok Kim[‡], Mughees Khan[‡], Philip Muñoz[*], Eric Mazur[*] & Joanna Aizenberg[*‡§]

[*]School of Engineering and Applied Sciences, Harvard University, Cambridge, MA 02138 [†]Department of Mechanical Engineering, Massachusetts Institute of Technology, Cambridge, MA, 02139 [‡]Wyss Institute for Biologically Inspired Engineering, Harvard University, Cambridge, MA 02138 [§]Corresponding authors

Submitted to Proceedings of the National Academy of Sciences of the United States of America

Recently, diffraction elements that reverse the color sequence normally observed in planar diffraction gratings have been found in the wing scales of the butterfly Pierella luna. Here, we describe the creation of an artificial photonic material mimicking this reverse color-order diffraction effect. The bio-inspired system consists of ordered arrays of vertically oriented micro-diffraction gratings. We present a detailed analysis and modeling of the coupling of diffraction resulting from individual structural components and demonstrate its strong dependence on the orientation of the individual miniature gratings. This photonic material could provide a basis for novel developments in bio-sensing, anti-counterfeiting and efficient light management in photovoltaic systems and light emitting diodes.

Bio-inspired optics | Micro-gratings | Biophotonics

Three-dimensional photonic crystals (1-5), materials with two-dimensional micro- or nano-sized periodic morphologies (6-8) and one-dimensional multilayer configurations (9) have been identified as the primary cause of structural coloration in a wide variety of non-related biological organisms. In contrast, surface-confined diffraction elements for the separation of incident light into specific colors are less abundant in nature and have only been discovered in a handful of organisms (10), including a fossil polychaete (7), the sea mouse *Aphrodita* sp. (6) and some flowering plants (11). Recently, diffraction elements that reverse the color sequence normally observed in planar diffraction gratings have been found in the scales of the butterfly *Pierella luna* (12).

Inspired by this biological light manipulation strategy, we devised an artificial material morphology mimicking the butterfly's diffraction effect by creating periodic arrays of vertically oriented individual micro-diffraction gratings. In addition to the butterfly-inspired reverse color order diffraction arising from each individual micro-grating, the periodicity between the individual gratings causes diffraction on a different length scale, leading to complex intensity distributions in experimentally measured angularly resolved reflection spectra. An in-depth analysis of the observed diffraction phenomenon complemented by optical modeling revealed a strong dependence of the optical signature on the orientation of the gratings. Such an effect can only be seen because of the hierarchical nature of the superposed, orthogonal grating features. To further elucidate the role of the different structural components for the emerging reflection spectra, the initially vertically oriented individual micro-gratings were subjected to a tilt, resulting in a predictable change of the surface's optical signature.

The dorsal side of the fore and hind wings of *P. luna* males are dull brown in diffuse ambient illumination (Fig. 1A, left). When exposed to directional illumination at grazing incidence, a coin-sized spot on each forewing displays an angle-dependent color variation across the whole visible spectrum (Fig. 1A, right). The color changes from red to blue with increasing observation angle unlike the variation from blue to red normally observed in conventional diffraction gratings (13). This reverse color diffraction effect results from the local morphology of individual scales within the colored spot on the fore wings (12). The top parts of the scales are curled upwards, orienting lines of periodically arranged cross-ribs perpendicular to the wing surface and the wing surface normal. (Fig. 1C,D). Light incident at an angle onto the curled parts of the scales is diffracted by the cross-rib structure acting as a diffraction grating, with a periodicity of ∼400nm. The alignment of the grating perpendicular to the surface results in the reverse color sequence that can be observed in angularly resolved reflection spectra and in the diffraction pattern (Fig. 1E,F).

The identification of this unusual diffraction effect on the wings of *P. luna* (12) provided inspiration for the development of a bio-inspired photonic system that incorporates vertically oriented micro-diffraction gratings with sub-micrometer periodicity analogous to the key features observed in the natural structure. In addition, the artificial system displays a periodic arrangement of the individual vertical gratings in large arrays with two-dimensional micro-scale periodicity. This structural feature, which is not found in the natural organism, enriches the optical signature of the artificial system via coupling of the diffractive modes of the two present hierarchical morphologies. In the following, we discuss the optical properties of the artificial system and demonstrate that the modification of either one of the grating morphologies changes the diffraction signature in predictable ways.

Significance

In the course of evolution, many organisms have developed unique light manipulation strategies that rely on intriguing combinations of a broad range of optical effects generated by materials with sophisticated multi-scale hierarchical structural arrangements. By exploiting the optical principles underlying natural structural color, we can generate new photonic materials. Researchers have only just begun to match nature's morphological and compositional complexity in man-made materials using nanofabrication. We present a bioinspired photonic material that mimics the reverse color order diffraction found in the butterfly Pierella Luna. Exploiting and improving the butterfly's strategy, we create new photonic materials that increase our basic understanding of the optical interplay of hierarchical structures and provide a platform for the development of novel photonic devices.

Reserved for Publication Footnotes

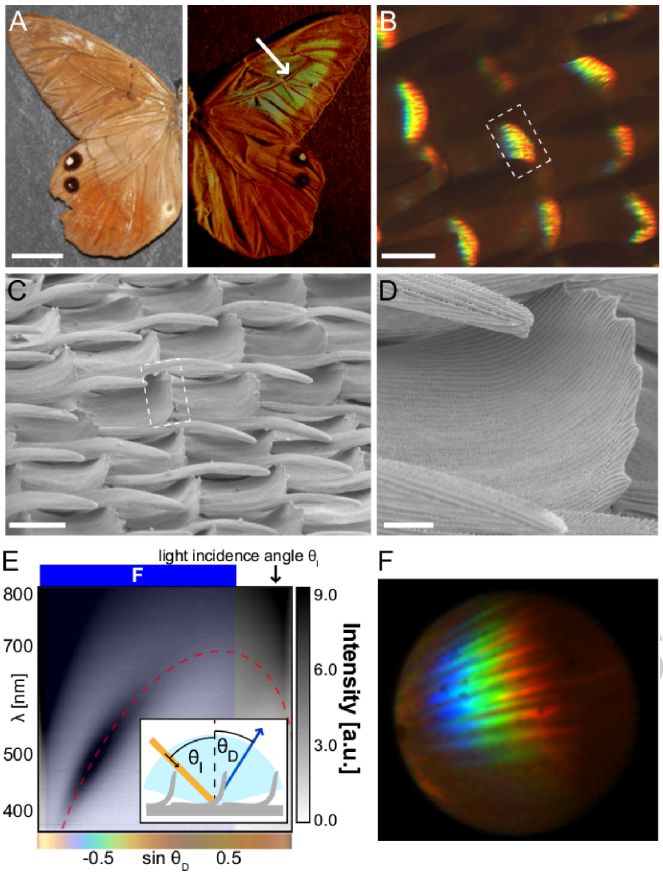

Fig. 1. Optical properties of the curled scales in buttery *Pierella luna*. **A**, Optical image of *P. luna* under diffuse lighting (left) and directional lighting at grazing incidence (right). Scale bar 10 mm. **B**, Optical micrograph of *P. luna* scales under oblique illumination. Scale bar 50 µm. **C**, Scanning electron micrograph (SEM) of scales in the colored wing region. Scale bar 50 µm. White dashed boxes in (B) and (C) mark the curled tops of the scales from which the color originates. **D**, Close-up image of the curled region of the scale from which the color originates. Scale bar 20 µm **E**, Gray-scale encoded reflection intensity as a function of wavelength and propagation direction showing the inverse color order diffraction pattern for 65° light incidence. The red dashed line indicates the predicted location of the diffraction due to the cross-rib structures for an orientation of the curled scale sections of -25° relative to the surface normal and a cross-rib periodicity of 390 nm. The blue shaded region signifies the angle range for which the diffraction microscopy image of curled P. luna scales in (F) was obtained. The color bar under the graph shows the human-eye perceived color for the spectra observed at the corresponding angles calculated by the CIE 1931 standards [18]. **F**, Diffraction microscopy image of the colored spot of a P. luna wing showing multiple diffracted orders in similar angular locations due to the variation in the position and angle of the diffracting scales.

The artificial system consists of an array of individual 10 µm long, 2 µm wide and 18 µm high plates arranged in rows with an inter-plate spacing of 10 µm and a separation of 5 µm between individual rows of plates (Fig. 2A). These parameters result in an overall periodicity of 12 µm in the direction perpendicular to the plates and 15 µm in the direction collinear with the plane of the plates and the sample surface. A periodic wave pattern—termed "scallops"—of ~500nm pitch runs along the sides of each individual plate (Fig. 2B).

The bio-inspired diffraction elements are fabricated in a double-molding procedure. Starting from a silicon master, a periodic array of scalloped micro-plates is first cast into polydimethylsiloxane to form a negative mold (14), which is then replicated with a UV-curable epoxy to produce a positive replica of the master silicon structure with the original scallops on the individual plates well preserved. The silicon master is formed using the Bosch process (15), in which multiple etching and passivation steps give rise to the periodic undulations on the micro-plate surface. The pitch and height of these grating structures can be controlled by adjusting the etching parameters (16, 17). Here, they are chosen to be comparable to the spacings and dimensions of the diffraction-inducing micro-ribs on the *P. luna* scales (Fig. 2B), and hence are expected to cause a similar diffraction effect.

It is important to notice that in the biological system, the periodicity of the diffraction grating-supporting scales is of the order of 80 ± 10 µm along their length and 60 ± 10 µm perpendicular to the scale axis (Fig. 1B). Due to these large distances between diffraction elements and a non-negligible amount of irregularity in the location of individual scales, no coherence is observed for light diffracted from adjacent scales. The overall color splitting only results from the diffraction caused by the cross-rib gratings on the individual scales, which is confirmed by variable angle spectroscopy and by diffraction microscopy measurements (Fig. 1D). Unlike in the biological system, the individual micro-diffraction gratings in the artificial system are intentionally arranged in a highly periodic manner, which is expected to result in a richer diffraction signature and provide additional possibilities of tailoring the interaction of light beyond the diffraction induced by the scallops on the plates.

Variable observation-angle spectroscopy performed on the artificial system serves to spectrally and angularly resolve parts of the complex diffraction pattern (Fig. 2C). For each measurement the plane of light incidence is chosen to be perpendicular to the surface of the individual micro-plates. The light incidence angle θ_I is fixed and the observation angle θ_D is varied in the plane of light incidence to capture light reflected in an angular range of ±75° around the sample surface normal. Two main features are observed in these measurements:

(1) Straight lines of higher intensity resulting from diffraction caused by the inter-plate periodicity represent the individual diffraction orders; the experimentally observed locations of these diffraction orders (shown in Fig. 2C,H) can be directly calculated using the grating equation (13). An example of such a calculation can be seen in SFig. 1. Due to the large inter-plate pitch of 12 µm the angular separation between adjacent diffraction orders and the free spectral range of each individual order are small. For light incident at an angle $\theta_I = 45°$, eight positive propagating diffraction orders (left of the 0th order at $\sin(\theta) = -0.71$ in Fig. 2C) and 53 negative propagating orders are captured with the highest intensity in the direct reflection (0th order) and in the adjacent orders.

(2) There is an arc-shaped distribution of intensity maxima across different diffraction orders (emphasized by dashed red lines in Fig. 2C).

This anomalous redistribution of light in the diffraction orders is caused by the scallops on each individual plate. To properly describe the diffraction resulting from the micro-diffraction gratings oriented normally to the substrate, the grating equation (13) has to be reformulated taking into account their vertical orientation for diffraction in the plane of the scallops:

$$[1]\quad \lambda = \frac{d}{m}(\cos\theta_I + \cos\theta_D),$$

where d is the grating periodicity, m is the diffraction order, θ_I is the light incidence angle and θ_D is the diffraction angle. This equation describes the arc shape-like pattern observed in the experiment under the assumption that the plates are vertical (Fig. 2C red shaded region).

Imaging of the diffraction patterns by diffraction microscopy provides a direct visualization of the effects observed in the variable-angle spectroscopy measurements. The angle range that can be visualized in these measurements is determined by the numerical aperture of the microscope objective. For a given light incidence angle θ_I the diffraction caused by the periodic ensemble

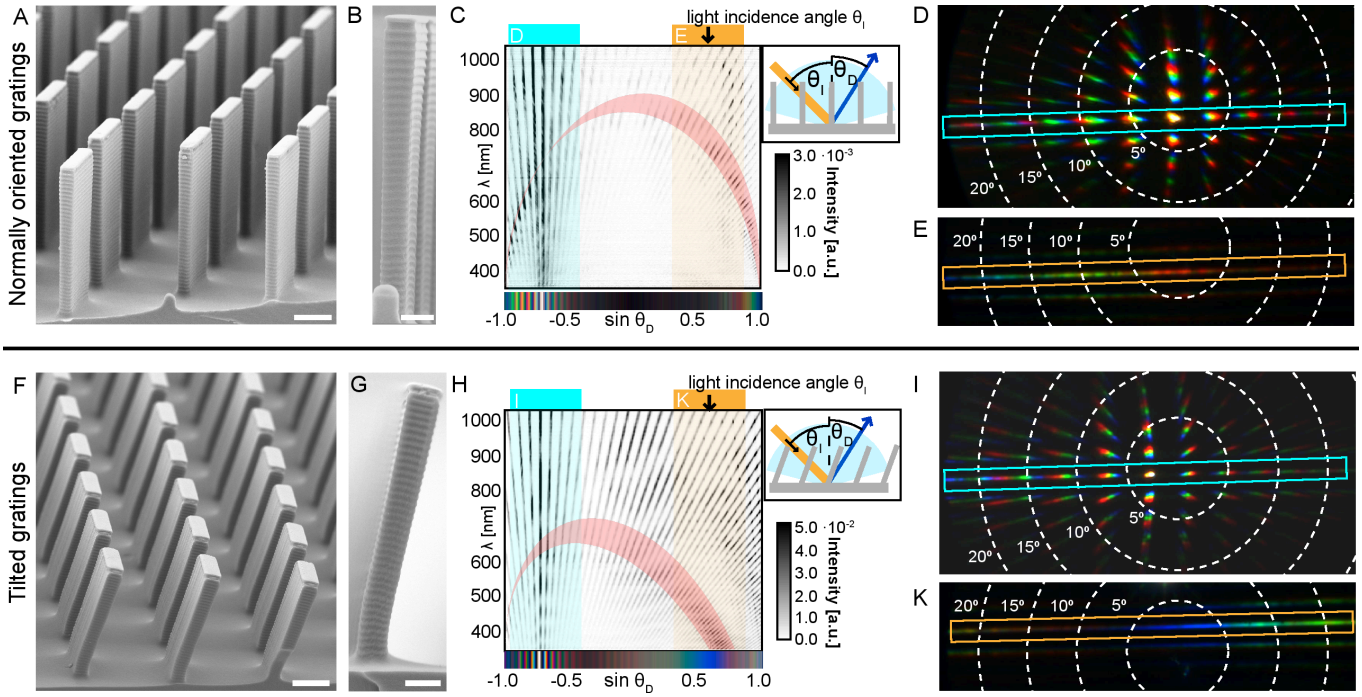

Fig. 2. Geometry and optical properties of the artificial photonic structure mimicking P. luna with vertically oriented (top row) and tilted (bottom row) diffraction gratings. **A**, SEM of the array of scalloped microplates. Scale bar 5 μm. **B**, SEM of an individual plate with regular scallops. Scale bar 2 μm. **C**, Variable angle spectroscopic data for 45° light incidence showing the arc-shaped diffraction pattern caused by the diffraction from the scallops coupled with the diffraction due to the plates. The measurement geometry is shown in the top right inset. The red overlay displays where the first diffraction order of the scallops based on the grating equation (eq. 2) is expected for tilt angles of –3° to 5°. The color bar under the graph shows the human-eye perceived color for the spectra observed at the corresponding angles calculated by the CIE 1931 standards (18). **D**, Diffraction pattern caused by the periodic ensemble of micro-plates for 45° light incidence. A choice of propagation angles is visualized by the white dashed lines. The diffraction orders within the blue frame correspond to the diffraction observed in the angular range marked in blue in (C). **E**, Diffraction pattern resulting from the scallops on individual plates. The diffraction orders within the yellow frame correspond to the diffraction observed in the angular range marked in yellow in (C). **F-K**, Same as (A-E), for tilted gratings. Red overlay in (H) marks the range where higher intensities are predicted by the grating equation for tilt angles between 19° and 27°.

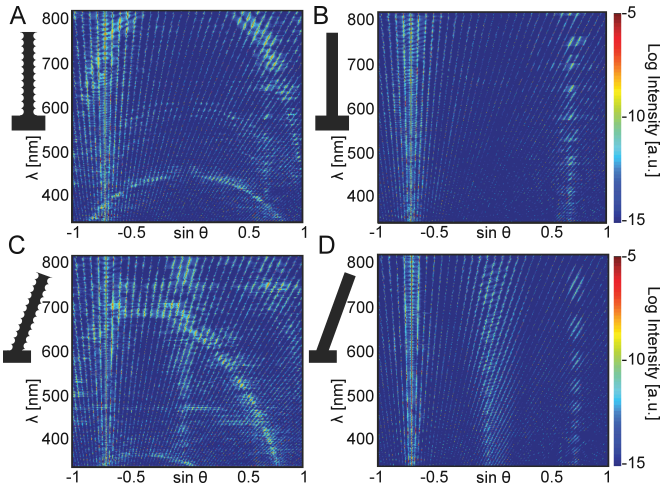

Fig. 3. Modeling of the expected diffraction patterns originating from the ordered array of gratings with 45° illumination. **A**, Calculated diffraction pattern for upright plates with scallops. **B**, Calculated diffraction pattern for upright plates without scallops. **C**, Calculated diffraction pattern for 23° tilted plates with scallops. **D**, Calculated diffraction pattern for 23° tilted plates without scallops.

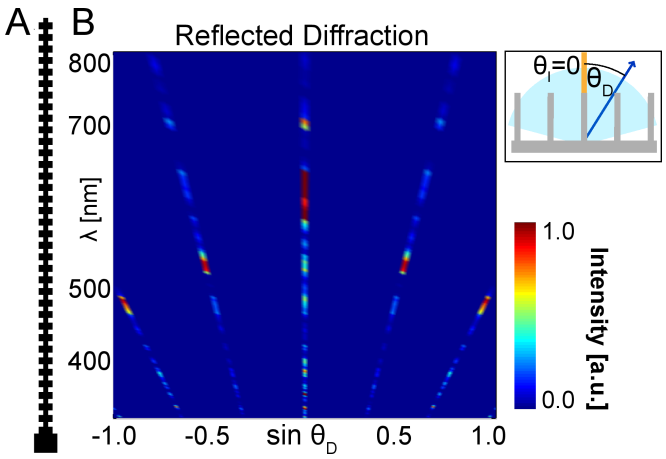

Fig. 4. Diffraction discretization. **A**,1 micron wide unit cell for diffraction grating simulated via FDTD. **B**, Reflected spectra calculated from FDTD simulation of (A) showing bright spots in each diffracted order with discrete jumps in the diffracted wavelength.

of plates is most clearly observed when collecting light with the objective's axis aligned with the specular reflection direction $\theta_D = -\theta_I$ (Fig. 2D, with the signal in the blue box corresponding to the blue shaded spectral range in Fig. 2C). Imaging of the sample's diffraction in the Littrow mounting (13), where light is incident on the sample through the microscope objective, allows for the capturing of the diffraction component induced by the scallops on the individual plates (Fig. 2E, with the signal in the yellow box corresponding to the yellow shaded spectral range in Fig. 2C). This feature is easily distinguished from the diffraction of the plate ensemble by the wider color spread.

Overall, the measurements provide clear evidence of coupling between the first order mode of the scallop diffraction and the

inter-plate periodicity based diffraction modes. The diffraction coupling can be controlled by adjusting the pitch of the scallops on individual plates and the inter-plate geometry in the manufacturing procedure. Likewise, a change in inclination of the micro-diffraction gratings with respect to the substrate is expected to be reflected in a variation of the diffraction patterns. This change can indeed be observed by imposing a controlled tilt of ~20° on the micro-plates by shearing the sample (Fig. 2F,G).

The bending leaves the locations of the diffraction modes resulting from the inter-plate periodicity largely unaffected. Only minor wavelength-dependent intensity variations in each diffraction mode are apparent (Fig. 2H,I). At large angles θ_D, measured from the sample surface normal, a region of higher reflection intensity appears, which is related to the inclination of the individual plates, i.e. the blaze of the grating array. By contrast, the diffraction caused by the scallops on the individual plates is strongly influenced by the variation in plate tilt angle shifting the observed arc-shaped pattern in wavelength and angular position (Fig. 2H,K). For micron-sized diffraction gratings which have a tilt angle, β, relative to the surface normal, the diffraction grating equation can be reformulated as:

[2] $\lambda = \frac{d}{m}(\cos(\theta_I - \beta) + \cos(\theta_D - \beta))$.

By calculating a fit for the arc-shaped intensity distribution across the different diffraction orders in the variable angle spectroscopic data (Fig. 2H, red shaded region), the tilt angle of the plates relative to the surface normal is found to be $\beta \approx 23°$, in agreement with the SEM image analysis.

These findings are further supported by Finite Difference Time Domain simulations (19). By comparing the plates with and without scalloping, the arc-shaped intensity distribution across diffraction orders is clearly identified as the diffraction resulting from the scallops (Fig. 3). Simulations of 23° tilted plates with 45° incident illumination show that this arc-shaped diffraction pattern gets skewed and spectrally shifted as predicted by Eq. 2 and observed in the experiments; the influence of the blaze of the regular array of individual gratings, separate from the effect of the scallops, can also be seen by closely examining Fig. 3 and noting that the two tilted plate simulations have regions of high intensity reflection at $\sin(\theta) \approx 0$ where the upright plates do not. Furthermore, the simulations serve to predict and optimize the influence of variations in inter-plate geometry, scallop grating pitch and shape and plate tilt angle prior to the manufacturing of the system.

While the angular positions of the diffraction modes resulting from the inter-plate periodicity only vary with the angle of light incidence θ_I; for a given θ_I the diffraction pattern caused by the regular scallops on individual plates is strongly affected by a change in tilt of the plates relative to the sample normal. Consequently, a means of reversibly varying the plate tilt angle can provide the possibility to dynamically tune the diffraction pattern independent of light incidence. Possible means of achieving such reversible actuation include embedding the plates in a stimuli-responsive hydrogel (20-23), using a soft material negative of the structure and applying shear force to bend the micro-gratings, modifying the tips of the plates with ferromagnetic particles to allow for dynamic reconfiguration of the plate geometry using magnetic fields (24), or implementing tuning mechanisms shown for simple planar diffraction gratings that rely on electric fields or mechanical deformation (25-28).

Biological strategies for light manipulation have already been successfully implemented in nanophotonic devices for applications in chemically selective vapor sensing, pH determination, infrared imaging, SERS-based chemical analysis, and localized heating from infrared absorption (29-34). The rich and tunable optical signature of our hierarchical bio-inspired diffraction-based photonic material platform could provide a basis for novel developments in bio-sensing (35-37), efficient light management in photovoltaic systems (38-40), enhanced light extraction and radiation profile shaping in light emitting diodes (41-43) and optically variable devices in consumer product design and anti-counterfeiting (44-46).

Our results demonstrate the versatility of a bio-inspired approach towards the creation of novel photonic systems. The unique diffraction-inducing nano- and micro-scale architecture previously discovered in the scales of the male butterfly *P. luna* served as inspiration for artificial micro-diffraction grating arrays. While our photonic system mimics the reverse diffraction color sequence found upon interaction of light with the butterfly's scales, it also provides additional complexity in the diffraction patterns due to a periodic arrangement of the diffraction elements not found in the natural structure. Such arrays provide a platform for hierarchical photonic systems displaying unique diffraction coupling. A detailed optical analysis and modeling of the diffraction patterns allowed us to observe, understand and decouple diffraction effects induced by the plate ensemble and by the regular scalloping of individual plates. A variation of the light incidence angle results in the expected shifting of the plate ensemble diffraction modes but does not affect the diffraction resulting from individual plates. On the other hand, a variation in plate inclination leaves the inter-plate geometry diffraction modes untouched but has a strong influence on the scallop-induced diffraction.

The intensity distribution of the diffraction induced by the scallops is modulated by the diffraction induced by the plate ensemble. Where the scallop diffraction arc coincides with a plate ensemble diffraction order a peak in intensity is observed. A decrease in the plate ensemble period would result in fewer propagating plate ensemble diffraction orders with a larger free angular range in between. This would lead to a discretization of the scallop diffraction pattern (seen in the FDTD simulation in Fig. 4) inducing a discrete and easily perceivable color variation with potential applications in the development of novel optically variable devices in security printing and consumer product labeling. Currently, efforts are underway to fabricate the diffraction structures in different material combinations that provide a higher refractive index contrast, thereby strengthening the diffractive signal.

Materials and Methods

Manufacture of artificial diffraction structures

When Bosch etching (15) is used in conjunction with photolithography, the multiple etching and passivation steps give rise to a periodicity in the sidewall of the structures due to the repeated underetching. While, typically, the goal of this etching method is to create vertical sidewalls, these undulations in the sidewall can form a diffraction grating similar to that on the *Pierella luna* scales if the periodicities are chosen to fall within the range of optical wavelengths.

Once structures with the correct geometry are created in silicon, they can be replicated in other materials with better optical properties by using soft lithographic methods (14). By using soft, transparent materials instead of silicon, the structures can be bent much more easily and the optical properties can be changed by applying metal coatings or doping the material with pigments or other materials with interesting optical properties. The replication is achieved by using a polydimethylsiloxane (PDMS) mold of the silicon master and curing an epoxy via UV light before removal from the mold.

Structural and optical analysis

Once scalloped plate structures are made, optical characterization is performed for comparison of the structures observed on *Pierella luna* and the fabricated systems. Several different types of characterization were employed, including variable-angle spectroscopy, diffraction microscopy, and scanning electron microscopy.

For the variable angle spectrometry setup, an Ocean Optics DH-2000 UV-VIS-NIR light source was used to illuminate a small spot (~1 mm) of the sample at a given incidence angle θ_I. For each angle of illumination, light was collected at half degree increments for –75° to +75° relative to the sample normal and spectrally analyzed using an Ocean Optics Maya Pro 2000 spectrometer.

For the diffraction microscopy images, a Bertrand lens was used to focus on the back focal plane of the objective of an upright BXFM Olympus optical microscope. The sample was illuminated either from an external source

oriented at a 90° angle to the microscope objective with a spot size larger than the sample field of view, or with a small diameter optical fiber coupled into the microscope light path (Littrow mounting).

Scanning electron microscopy images were taken on a Zeiss Ultra55 or a Zeiss Supra55VP SEM after coating the polymer structures with a thin layer of gold to prevent charging.

Optical modeling

Finite Difference Time Domain (47) methods were employed to numerically simulate the results obtained from the variable angle spectroscopy measurements. A commercial-grade simulator based on the finite-difference time-domain method was used to perform the calculations.(19) Perfectly matched layers (48) were used to prevent reflections from the top and bottom of the simulation cell, while Bloch boundary conditions were used for the sides of the simulation cell in order to model light scattering from a periodic array at non-normal incidence. To simulate broadband angled scattering, each simulation was repeated for a range of Bloch wavevectors, which were combined to produce scattered field profiles corresponding to an incidence angle of 45° ± 1° for wavelengths of 320-800 nm. Far field projections of the calculated local fields resulted in diffraction patterns (Fig. 3) analogous to the variable angle spectroscopic data.

The diffraction discretization FDTD simulation was similarly performed in MEEP, a free FDTD software.(49) The use of normal incidence illumination for this simulation allowed all frequencies and angles to be calculated without using a sweep of incidence angles.

Author contributions

Ma.K. and J.A. conceived the bio-inspired photonic system and supervised the research. G.E. and Ma.K. performed the studies of the natural structure. G.E., P.K and Mu.K. manufactured the micro-diffraction grating system. G.E. and Ma.K. performed the optical characterization. G.E., P.M., and Ma.K. performed the optical modeling. G.E., Ma.K. and J.A. wrote the manuscript. All authors discussed the results and commented on the manuscript.

Acknowledgments.

This work was supported by the U.S. Air Force Office of Scientific Research Multidisciplinary University Research Initiative under award number FA9550-09-1-0669-DOD35CAP. Ma.K. acknowledges the financial support from the Alexander von Humboldt Foundation in form of a Feodor-Lynen postdoctoral research fellowship. Vukusic, P., & Sambles, J. R. (2003). Photonic structures in biology. *Nature*, *424*(6950), 852–5. doi:10.1038/nature01941

Bibliography 1. Vukusic P, Sambles JR (2003) Photonic structures in biology. *Nature* 424(6950):852–855. 2. Parker AR, Welch VL, Driver D, & Martini N (2003) Structural colour: opal analogue discovered in a weevil. *Nature* 426(6968):786–787. 3. Galusha JW, Richey LR, Gardner JS, Cha JN, Bartl MH (2008) Discovery of a diamond-based photonic crystal structure in beetle scales. *Phys Rev E* 77(5):050904. 4. Saranathan V, et al. (2010) Structure, function, and self-assembly of single network gyroid (I4132) photonic crystals in butterfly wing scales. *Proc Natl Acad Sci USA* 107(26):11676–11681. 5. Simonis P, Vigneron JP (2011) Structural color produced by a three-dimensional photonic polycrystal in the scales of a longhorn beetle: *Pseudomyagrus waterhousei* (Coleoptera: Cerambicidae). *Phys Rev E* 83(1):011908. 6. Parker AR, McPhedran RC, McKenzie DR, Botten LC, Nicorovici NA (2001) Photonic engineering. Aphrodite's iridescence. *Nature*, 409(6816):36–37. 7. Trzeciak TM, Vukusic P (2009) Photonic crystal fiber in the polychaete worm Pherusa sp. *Phys Rev E*, 80(6):061908. 8. Prum RO, Torres R (2003) Structural colouration of avian skin: convergent evolution of coherently scattering dermal collagen arrays. *J Exp Biol* 206(14):2409–2429. 9. Welch V, Vigneron J, Lousse V, Parker A (2006) Optical properties of the iridescent organ of the comb-jellyfish Beroë cucumis (Ctenophora). *Phys Rev E* 73(4):041916. 10. Seago AE, Brady P, Vigneron JP, Schultz TD (2009) Gold bugs and beyond: a review of iridescence and structural colour mechanisms in beetles (Coleoptera). *J R Soc Interface* 6:S165–S184. 11. Whitney HM, et al. (2009) Floral iridescence, produced by diffractive optics, acts as a cue for animal pollinators. *Science* 323(5910):130–133. 12. Vigneron JP, et al. (2010) Reverse color sequence in the diffraction of white light by the wing of the male butterfly Pierella luna (Nymphalidae: Satyrinae). *Phys Rev E* 82(2):021903. 13. Palmer, C (2005) Diffraction Grating Handbook (Newport Corporation, Rochester, New York, USA). 14. Xia Y, Whitesides GM (1998). SOFT LITHOGRAPHY. *Annu Rev Mater Sci*, 28(1):153–184. 15. Plasma Polymerizing Temporary Etch Stop. Laermer, F. and Schilp, A., Patent US5501893. 1996. Print. 16. Ayón, AA, Braff RA, Bayt R, Sawin HH, Schmidt MA (1999). Influence of Coil Power on the Etching Characteristics in a High Density Plasma Etcher. *J Electrochem Soc*, 146(7), 2730. 17. Maluf N, Williams K (2004) Introduction to microelectromechanical systems engineering (Artech house publishers). 18. CIE (1931) Commission internationale de leclairage proceedings. 19. Lumerical Solutions, Inc. http://www.lumerical.com/tcad-products/fdtd/. 20. Bassil M, Davenas J, Tahchi ME (2008) Electrochemical properties and actuation mechanisms of polyacrylamide hydrogel for artificial muscle application. *Sens Actuators B Chem* 134(2):496–501. 21. Kim P, Zarzar LD, Zhao X, Sidorenko A, Aizenberg J (2010) Microbristle in gels: Toward all-polymer reconfigurable hybrid surfaces. *Soft Matter* 6(4):750-755. 22. Kim P, Zarzar LD, He X, Grinthal A, Aizenberg J (2011) Hydrogel-actuated integrated responsive systems (HAIRS): Moving towards adaptive materials. *Curr Opin Solid State Mater Sci* 15(6):236–245. 23. DeVolder M, Tawfick SH, Copic D, Hart AJ (2011) Hydrogel-driven carbon nanotube microtransducers. *Soft Matter* 7(21):9844-9847. 24. Sniadecki NJ, et al. (2007) Magnetic microposts as an approach to apply forces to living cells. *Proc Natl Acad Sci USA* 104(37):14553–14558. 25. Aschwanden M, Stemmer A (2006) Polymeric, electrically tunable diffraction grating based on artificial muscles. *Opt Lett* 31(17):2610-2612. 26. Schueller OJ, Duffy DC, Rogers JA, Brittain ST, Whitesides GM (1999) Reconfigurable diffraction gratings based on elastomeric microfluidic devices. *Sens Actuators A Phys* 78(2-3):149–159. 27. Xia Y,et al. (1996) Complex Optical Surfaces Formed by Replica Molding Against Elastomeric Masters. *Science* 273(5273):347–349. 28. Butler MA, et al. (2001) A MEMS-based programmable diffraction grating for optical holography in the spectral domain. *Int Electron Devices Meeting. Technical Digest* (pp. 41.1.1–41.1.4). IEEE. 29. Potyrailo, RA, et al. (2007) Morpho butterfly wing scales demonstrate highly selective vapour response. *Nat Photonics* 1(2):123–128. 30. Garrett NL, et al. (2009) Spectroscopy on the wing: naturally inspired SERS substrates for biochemical analysis. *J Biophotonics* 2(3):157–166. 31. Pris, AD, et al. (2012) Towards high-speed imaging of infrared photons with bio-inspired nanoarchitectures. *Nat Photonics* 6(3):195–200. 32. Zang X, Tan Y, Lv Z, Gu J, Zhang D (2012) Moth wing scales as optical pH sensors. *Sens Actuators B Chem* (166-167):824–828. 33. Potyrailo RA, et al. (2013) Discovery of the surface polarity gradient on iridescent Morpho butterfly scales reveals a mechanism of their selective vapor response. *Proc Natl Acad Sci USA* 110(39):15567–15572. 34. Kim, S, et al. (2012) Silk inverse opals. *Nat Photonics* 6(12):818–823. 35. Lawrence CR, Geddes NJ, Furlong DN, Sambles JR (1996) Surface plasmon resonance studies of immunoreactions utilizing disposable diffraction gratings. *Biosens Bioelectron* 11(4):389–400. 36. Dostálek J, Homola J, Miler M (2005) Rich information format surface plasmon resonance biosensor based on array of diffraction gratings. *Sens Actuators B Chem* 107(1):154–161. 37. Wark AW, Lee HJ, Qavi AJ, Corn, RM (2007) Nanoparticle-enhanced diffraction gratings for ultrasensitive surface plasmon biosensing. *Anal Chem* 79(17):6697–6701. 38. Heine C, Morf RH (1995) Submicrometer gratings for solar energy applications. *Appl Opt 34*(14):2476–2482. 39. Feng N-N, et al. (2007) Design of Highly Efficient Light-Trapping Structures for Thin-Film Crystalline Silicon Solar Cells. *IEEE Trans Electron Devices* 54(8):1926–1933. 40. Munday JN, Atwater HA (2011) Large integrated absorption enhancement in plasmonic solar cells by combining metallic gratings and antireflection coatings. *Nano Lett* 11(6):2195–2201. 41. Fujita M, et al. (2005) Optical and Electrical Characteristics of Organic Light-Emitting Diodes with Two-Dimensional Photonic Crystals in Organic/Electrode Layers. *Jpn J Appl Phys* 44(6A):3669–3677. 42. Wierer JJ, Jr, David A, Megens MM (2009) III-nitride photonic-crystal light-emitting diodes with high extraction efficiency. *Nat Photonics* 3(3):163–169. 43. Arpin KA, et al. (2010) Multidimensional architectures for functional optical devices. *Adv Mater* 22(10):1084–1101. 44. vanRenesse RL (1997) Paper based document security: a review. *Security and Detection*. ECOS 97:75 -80. 45. Staub R, Tompkin WR (1998) Nonstandard diffraction structures for ovds. *Proc SPIE* 3314:194-202. 46. Lee RA (2000) Micro-technology for anti- counterfeiting. *Microelectron Eng.* 53(1-4):513-516. 47. Yee K (1966) Numerical solution of initial boundary value problems involving Maxwell's equations in isotropic media. *IEEE Trans Antennas Propag* 14(3):302-307. 48. Berenger J-P (1994) A perfectly matched layer for the absorption of electromagnetic waves. *J Comput Phys* 114(2):185-200. 49. Oskooi AF, et al. (2010) Meep: A flexible free-software package for electromagnetic simulations by the fdtd method. *Comput. Phys. Commun.* 181: 687-702.